MOLECULAR
METABOLISM

Functional peroxisomes are required for β-cell integrity in mice

Ritesh Kumar Baboota [1,5], Abhijit Babaji Shinde [1,5], Katleen Lemaire [2], Marc Fransen [3], Stefan Vinckier [4],
Paul P. Van Veldhoven [3], Frans Schuit [2], Myriam Baes [1,*]

ABSTRACT

Objectives: Peroxisomes play a crucial role in lipid and reactive oxygen species metabolism, but their importance for pancreatic β-cell functioning is presently unknown. To examine the contribution of peroxisomal metabolism to β-cell homeostasis in mice, we inactivated PEX5, the import receptor for peroxisomal matrix proteins, in an inducible and β-cell restricted manner ($Rip\text{-}Pex5^{-/-}$ mice).
Methods: After tamoxifen-induced recombination of the *Pex5* gene at the age of 6 weeks, mice were fed either normal chow or a high-fat diet for 12 weeks and were subsequently phenotyped.
Results: Increased levels of very long chain fatty acids and reduced levels of plasmalogens in islets confirmed impairment of peroxisomal fatty acid oxidation and ether lipid synthesis, respectively. The $Rip\text{-}Pex5^{-/-}$ mice fed on either diet exhibited glucose intolerance associated with impaired insulin secretion. Ultrastructural and biochemical analysis revealed a decrease in the density of mature insulin granules and total pancreatic insulin content, which was further accompanied by mitochondrial disruptions, reduced complex I activity and massive vacuole overload in β-cells. RNAseq analysis suggested that cell death pathways were affected in islets from HFD-fed $Rip\text{-}Pex5^{-/-}$ mice. Consistent with this change we observed increased β-cell apoptosis in islets and a decrease in β-cell mass.
Conclusions: Our data indicate that normal peroxisome metabolism in β-cells is crucial to preserve their structure and function.

1. INTRODUCTION

Peroxisomes are still enigmatic organelles six decades after their discovery [1]. The foremost metabolic functions of peroxisomes include α- and β-oxidation of fatty acids, synthesis of ether phospholipids, bile acids, and polyunsaturated fatty acids, and detoxification of oxygen radicals and glyoxylate [2]. More recently, it was discovered that peroxisomes also serve as a platform in antiviral signaling [3], and it is becoming clear that they have multiple interactions with other cellular organelles [4—6].

Whereas the role of peroxisomes has been intensively studied in tissues like liver and brain, their importance for pancreatic β-cell function remains largely unexplored. Intriguingly, pancreatic β-cells are almost devoid of catalase, a key peroxisomal antioxidant marker enzyme [7], due to islet-selective repression of the catalase gene [8]. Catalase belongs to a small group of 'forbidden' genes, that are thought to be suppressed in order to allow specific β-cell function [9,10]. However, individual overexpression of the 'disallowed' anti-oxidant enzymes, including catalase, in the cytosol or mitochondria did not impair responsiveness of insulin-secreting cells to glucose, leaving the functional importance of the suppression unresolved [11]. It was further reported that the frequency of diabetes is higher in catalase-deficient patients [12].

It is widely accepted that, in addition to oxidative stress, β-cells are susceptible to glucolipotoxicity [13]. Besides other mechanisms that were proposed, Lenzen and coworkers showed that H_2O_2 produced during peroxisomal β-oxidation is the mediator of fatty acid-induced toxicity in β-cells [14]. Treatment of RINm5F rat insulinoma cells and primary rat islets with various saturated fatty acids induced peroxisomal H_2O_2 production, as detected by peroxisome-targeted HyPer, a genetically encoded H_2O_2 sensor. Furthermore, the palmitate-induced cytotoxicity in RINm5F cells was rescued by

[1]KU Leuven — University of Leuven, Department of Pharmaceutical and Pharmacological Sciences, Laboratory of Cell Metabolism, B-3000, Leuven, Belgium [2]KU Leuven — University of Leuven, Department of Cellular and Molecular Medicine, Gene Expression Unit, B-3000, Leuven, Belgium [3]KU Leuven — University of Leuven, Department of Cellular and Molecular Medicine, Laboratory for Lipid Biochemistry and Protein Interactions, KU Leuven, B-3000, Leuven, Belgium [4]VIB-KULeuven Centre for Cancer Biology, Laboratory of Angiogenesis and Vascular Metabolism, B-3000, Leuven, Belgium

[5] Ritesh Kumar Baboota and Abhijit Babaji Shinde authors contributed equally.

*Corresponding author. Department of Pharmaceutical and Pharmacological Sciences, Laboratory of Cell Metabolism, Campus Gasthuisberg O/N2, Herestraat 49, B-3000, Leuven, Belgium. E-mail: Myriam.Baes@kuleuven.be (M. Baes).

Original Article

overexpression of catalase in peroxisomes or in the cytosol, but not in mitochondria [14].

A different perspective on the potential role of peroxisomal β-oxidation in β-cells was provided by a study from Hellemans et al. [15]. These authors showed that palmitate-induced β-cell toxicity was attenuated by the induction of both peroxisomal and mitochondrial β-oxidation using PPARα and retinoid X receptor agonists [15]. This points to a protective role of peroxisomal β-oxidation in insulin-producing cells. Together, these studies indicate that there are still uncertainties and different opinions about the potential role of peroxisomal metabolism in β-cell functioning. In the present study, we first assessed the abundance of peroxisomes in the endocrine pancreas. Subsequently, we used an *in vivo* loss-of-function approach to investigate the role of peroxisomes in pancreatic β-cells. Hereto, the import receptor PEX5, necessary for import of nearly all peroxisomal enzymes into the organelle, was targeted in a β-cell-restricted and inducible manner in adult mice resulting in functional peroxisome deficiency in β-cells.

2. METHODS

2.1. Generation of *Rip-Pex5*$^{-/-}$ mice

β-cell selective *Rip-Pex5*$^{-/-}$ mice were generated by mating *Pex5*$^{FL/FL}$ mice with tamoxifen-inducible Tg (Ins2-cre/ERT)^{1Dam} mice commonly known as *Rip(rat insulin promotor)-Cre/ER* mice [16] in a C57Bl6 background to obtain *Rip-Cre*$^+$*Pex5*$^{FL/WT}$, which were then crossed with *Pex5*$^{FL/FL}$ mice to obtain *Rip-Cre*$^+$*Pex5*$^{FL/FL}$ knockout mice *(denoted as Rip-Pex5*$^{-/-}$). Littermates carrying *Pex5*$^{FL/FL}$ without CRE expression *were* used as controls. Since *Rip-Cre* transgenic mice have been suggested to show glucose intolerance [17], *Rip-Cre*$^+$*Pex5*$^{WT/WT}$ and *Rip-Cre*$^+$*Pex5*$^{FL/WT}$ mice were also used as control for glucose intolerance experiments. Recombination was induced by intraperitoneal administration of 5 doses of 4 mg tamoxifen dissolved in corn oil on alternate days starting at the age of 6 weeks. Only male *Rip-Pex5*$^{-/-}$ mice were used for phenotypic analysis. Tamoxifen was also administered to littermate *Pex5*$^{FL/FL}$ mice which were used as controls. Subsequently, *Rip-Pex5*$^{-/-}$ mice and littermate controls were housed in groups of 3–5 and were fed either a normal chow or a HFD containing 45% kcal fat (D12451, Research Diets, NJ, USA) *ad libitum*; starting at the age of 8 weeks. All mice were bred in the conventional animal housing facility of the KU Leuven, had *ad libitum* access to water and were kept on a 12 h light and dark cycle. All animal experiments were performed in accordance with the "Guidelines for Care and Use of Experimental Animals" and fully approved by the Research Ethical Committee of the KU Leuven. No randomization was carried out and experimenters were not blinded to group assignment and outcome assessment.

2.2. Intraperitoneal glucose and insulin tolerance tests

Intraperitoneal glucose tolerance tests (IPGTT) and intraperitoneal insulin tolerance tests (IPITT) were performed in 20-week-old control and *Rip-Pex5*$^{-/-}$ mice either fed normal chow or a HFD diet for a period of 12 weeks. Mice were fasted either overnight for IPGTT or for 4–6 h for IPITT. Blood glucose levels and body weight were monitored after fasting and then mice were given an intraperitoneal injection of either 2 g D-glucose (IPGTT) or 0.75 U insulin (IPITT) per kg body weight. Blood glucose levels were measured at 6, 12, 30, 60, 120, 150, and 180 min for IPGTT and at 5, 10, 20, 30, 60, 90, and 120 min for IPITT following administration of glucose and insulin, respectively, with an Accu-Check® Aviva glucometer (Roche, Vilvoorde, Belgium). To quantify insulin, approximately 50 μl of blood was collected from each mouse before and after 6 and 12 min of glucose injection from the lateral tail vein, followed by separation of plasma and measured

using the Crystal Chem ultra-sensitive mouse ELISA kit (Downers Grove, IL, U.S.A.) according to the manufacturer's protocol (but 10 μl instead of 5 μl plasma was used).

2.3. *Ex vivo* insulin release

Islets were isolated using the collagenase perfusion method and glucose-stimulated insulin secretion (GSIS) was performed as described [18,19] with minor modifications. Briefly, isolated islets were allowed to recover for 3 h in RPMI1640 medium (Gibco, Invitrogen, UK) containing 10% fetal bovine serum and 100-U/mL penicillin-streptomycin at 37 °C under a humidified atmosphere of 5% CO_2 and 98% air. For insulin secretion studies, a batch of 50 size-matched islets was pre-incubated in HEPES Krebs buffer (KRBB) solution containing 5 mM glucose and 0.5% BSA for 30 min. Subsequently, islets were incubated consecutively in KRBB with 5 mM glucose for 1 h and in KRBB with 20 mM glucose for 1 h. All steps were performed at 37 °C in a tissue culture incubator. The supernatants were collected to measure insulin release and islets were then sonicated for 3 min in acidic ethanol (final concentrations: 75% EtOH, 0.1 N HCl, 1% Triton) for determining total insulin content. Samples were stored at −20 °C until further use. Insulin concentrations of these samples were determined using an ultrasensitive mouse insulin ELISA kit (Mercodia, Uppsala, Sweden) according to the manufacturer's protocol. The stimulation index is represented as the ratio of insulin secreted in response to high glucose versus insulin secreted under low glucose conditions [20].

2.4. Total pancreatic insulin content

Pancreata were dissected, and their weights were recorded. They were put into 5 ml cold (−20 °C) acidic ethanol (75% ethanol, 0.1 N HCl). After sonication (Soniprep 150, MSE, London, UK) for 2 min on ice, the homogenates were stored at −20 °C overnight. The next day the homogenates were spun at 3000 rpm for 10 min and the supernatants were collected for analysis of insulin content using the Crystal Chem ultra-sensitive mouse ELISA kit (Downers Grove, IL, U.S.A.) according to the manufacturer's protocol.

2.5. Immunohistochemical staining and morphometric analysis

Mice were anesthetized with a mix of Dormitor (1 mg/kg) and Nimatek (75 mg/kg) and subsequently perfused transcardially with PBS (pH 7.4) followed by 4% paraformaldehyde (PFA). Pancreata were isolated, post-fixed with 4% PFA overnight, and kept in 70% ethanol prior to paraffin embedding and sectioning (7 μm). The paraffin sections were deparaffinized and rehydrated using routine protocols. Sections were then treated with citrate buffer in a microwave oven to expose the antigenic sites. Blocking was done using

Antibody	Dilution	Manufacturer	Reference/catalog no.	Characteristics
Rabbit PEX14	1:200	—	[21]	Polyclonal
Rabbit ACAA1	1:100	—	[22]	Polyclonal
Rabbit Ki67	1:500	Thermo Scientific	PA5-19462	Polyclonal
Rabbit 4-HNE	1:200	Calbiochem	393207	Polyclonal
Rabbit LAMP2	1:200	GeneTex	GTX63319	Monoclonal
Mouse Insulin	1:2500	Abcam	Ab6995	Monoclonal
Anti-mouse IgG HRP	1:200	Agilent	P0447	Secondary antibody
Anti-rabbit IgG HRP	1:200	Agilent	P0448	Secondary antibody

Table 1 — Primary antibodies used for immunohistochemistry.

2% (v/v) normal goat serum in blocking buffer (0.1 M Tris-HCl pH 7.5, 0.15M NaCl, 0.5% (w/v) blocking reagent (Perkin Elmer, Waltham, USA) for 1h at room temperature to block non-specific binding sites followed by overnight incubation at 4 °C with primary antibodies (Table 1). For insulin single staining, sections were incubated overnight at 4 °C with the primary antibody followed by 1 h incubation with anti-mouse IgG HRP (Agilent, Burlingame, CA, USA). The TSA Cyanine 3 system (Perkin Elmer) was used for detection and nuclei were visualized with DAPI included in the mounting medium (Agilent). For double immunolabeling, the staining, which was detected with anti-rabbit IgG HRP (Agilent) and the TSA-Plus Fluorescein System (Perkin Elmer), was done first. To examine apoptotic cells, terminal deoxynucleotidyltransferase-mediated dUTP nick end labeling (Roche Applied Science, Indianapolis, IN, USA) was performed according to the manufacturer's protocol. These stainings were followed by insulin staining as described above.

For morphometric analysis, six sections separated by 200 μm were taken throughout the length of the pancreas and stained for insulin. Quantification of β-cell mass and islet size was done as described [23]. To quantify β-cell proliferation and apoptotic cell death, images of insulin-positive cells (20—25 islets per mouse; n = 5 per genotype) that stained with either Ki67 or TUNEL were captured and the percentage of proliferating or apoptotic cells was determined by counting the Ki67/TUNEL-positive nuclei among 150—300 β-cells per islet. Images for PEX14/ACAA1-stained sections were acquired using a Zeiss LSM 780 confocal microscope (Carl Zeiss, Munich, Germany), whereas other stainings were quantitatively assessed using a motorized inverted IX-81 microscope connected to a CCD-FV2T digital camera (Olympus, Aartselaar, Belgium).

2.6. Electron microscopy

The ultrastructure of pancreatic β-cells was examined using JEM1400 (JEOL) transmission electron microscopy (TEM). Briefly, mice were perfused with and subsequently, pancreas fragments were immersed in 2.5% glutaraldehyde buffered with 0.05 M Na-cacodylate buffer (pH 7.3) for 24 h. Prior to embedding in Agar 100 resin, samples were post-fixed in 2% osmium tetroxide (buffered with 0.05 M sodium cacodylate, pH 7.3) and dehydrated using acetone. After dehydration, ultrathin sections were prepared using a Reichert Jung Ultracut E microtome and stained with 0.1% thionin — 0.1% methylene blue. Ultrathin (±70 nm) sections were mounted on copper grids and stained with uranyl acetate and lead citrate before imaging. To quantify the number of altered mitochondria according to criteria described previously [24], the data obtained from a minimum of 35 independent β-cells from 3 to 4 mice per genotype was averaged. Similarly, 38 independent β-cells from 4 Rip-Pex5$^{-/-}$ mice were visualized to quantify the β-cells having vacuoles and subsequently, the number of vacuoles in those β-cells were counted and averaged.

2.7. Complex 1 enzyme activity measurement

Isolated islets were homogenized in extraction buffer and lysates (corresponding to 20 μg of proteins) were used to determine the complex I activity using the complex I enzyme activity dipstick assay kit (Abcam, Cambridge, UK) according to the manufacturer's protocol. Measurement of the protein concentration in cell lysates was performed using the Pierce BCA protein kit (Thermo Scientific, Rockford, IL, USA). Signals on the dipsticks were visualized using the ChemiDoc MP system (Bio-Rad; California, USA) and signal intensities were quantified with Image Lab software (Bio-Rad; California, USA).

2.8. Biochemical analyses

For C26:0-lysophosphatidylcholine (LPC) analysis, 150—300 islets were suspended in 400 μl PBS and homogenized by sonication. Fifty μl of each sample was set aside for protein determination, the rest was processed as described [25].

For plasmalogen analysis, 120—300 islets were extracted as described [26], and lipid extracts were analyzed for phospholipids [26] and plasmalogens. For the latter, acid-released aldehydes were derivatized into fluorescent decahydroacridine derivatives (adapted from [27]), which were separated by RP-HPLC (Waters Symmetry C18, 5 μm, 100 Å, 4.6 × 150 mm column) and monitored by fluorescence (Waters 2475 Multi-wavelength Fluodetector; ex 390 nm/em 460 nm) (Van Veldhoven P.P., unpublished data). Values were normalized to the phospholipid content of the extracts.

For western blotting, 150—200 islets were washed with ice-cold PBS and then lysed with buffer containing 50 mM Tris (pH 8), 150 mM NaCl, 1% NP40, and 1 mM EDTA. PEX5 [28] and ACAA1 [22] were detected using polyclonal rabbit antibodies in combination with HRP-labeled secondary antibodies and the ECL plus detection kit (GE Healthcare, Buckinghamshire, UK).

2.9. RNA sequencing and bioinformatics analysis

RNA was extracted from freshly isolated islets of HFD-fed control and Rip-Pex5$^{-/-}$ mice using the PureLink® RNA Mini Kit (ThermoFisher Scientific, Waltham, MA) following the manufacturer's protocol. RNA integrity was verified on the Agilent Bioanalyser (Agilent, Santa Clara, CA, USA) with the RNA nanochip. The RNA-seq libraries were prepared using the Illumina TruSeq RNA sample preparation kit following the manufacturer's instructions. After library construction, all libraries were quantified, pooled and sequenced on an Illumina NextSeq 500 platform using a 50 bp single-end protocol. After alignment of the sequencing reads to the mouse genome, quantification of transcript abundances was performed using the Kallisto software [29]. We performed a trimmed mean of M-values (TMM)-normalization using the R-package EdgeR [30] and normalization using Limma before down-stream differential analysis. Gene set enrichment analysis (GSEA) against the KEGG database was used to analyze pathway enrichment.

2.10. Statistical analyses

Statistical analyses were done using GraphPad Prism 5.01 software. Depending on the experimental design, statistical significance was determined by performing either unpaired t-test or one-way ANOVA followed by the Bonferroni test. Data are expressed as mean ± SEM. $P < 0.05$ was considered statistically significant.

3. RESULTS

3.1. Peroxisomes are abundant in the endocrine pancreas

Because of the low expression of catalase, the traditional peroxisomal marker enzyme, in pancreatic β-cells [7], we visualized peroxisomes in mouse whole pancreas sections by immunohistochemical staining using antibodies to PEX14, an essential peroxisomal membrane protein. Co-staining with insulin revealed that PEX14 immunoreactivity was markedly higher in the endocrine than in the exocrine pancreas (Figure 1A), pointing to an important function of peroxisomes in islets. Likewise, the peroxisomal β-oxidation enzyme ACAA1 was more abundantly expressed in islets, including β-cells, as compared to the surrounding cells (Figure 1A), which is indicative of an active peroxisomal β-oxidation pathway in insulin-producing cells. This observation
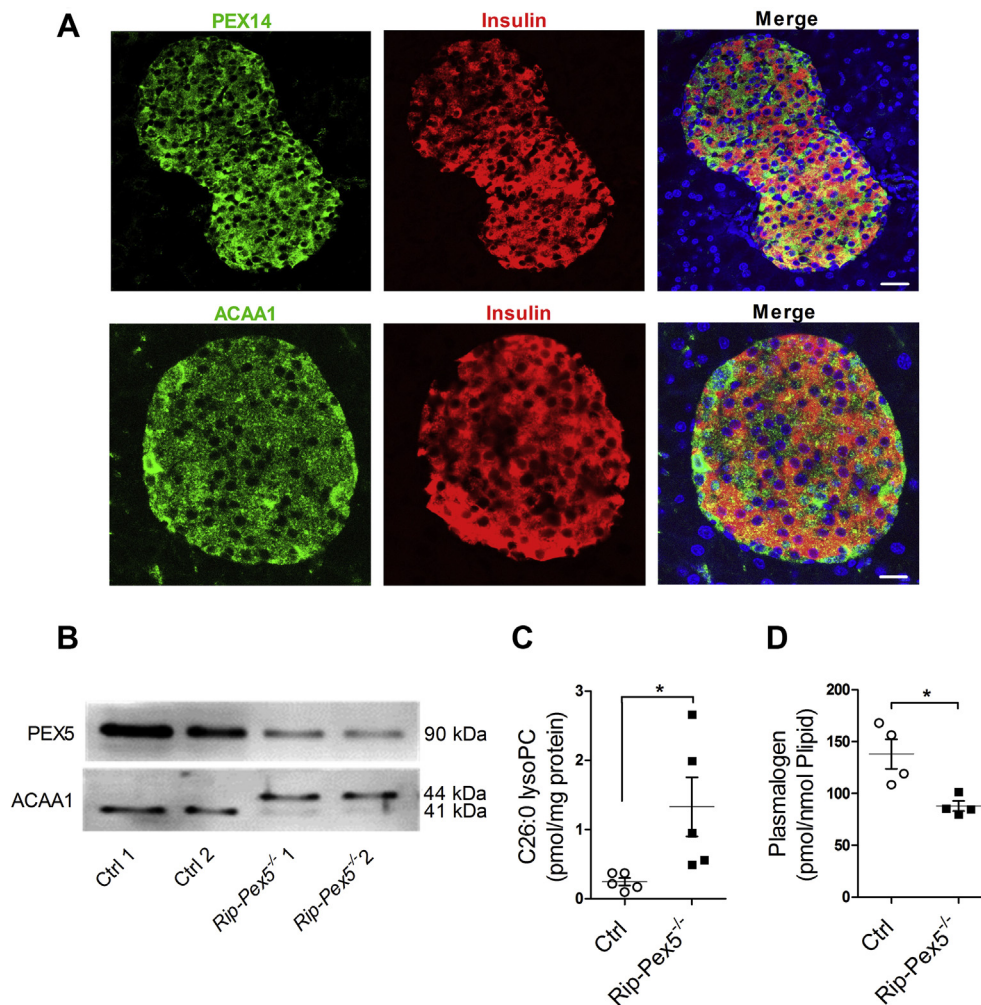
Figure 1: Peroxisome abundance in endocrine pancreas and validation of *Pex5* inactivation in islets of *Rip-Pex5*$^{-/-}$ mice. (A) PEX14 and ACAA1 staining (green) reveals the typical punctate appearance of peroxisomes that is more abundant in endocrine (colocalization with insulin, red) than in exocrine pancreas. Scale bars, 20 μm. **(B)** Western blot analysis of PEX5 and ACAA1 protein in islets of control and *Rip-Pex5*$^{-/-}$ mice. ACAA1 occurs in the processed 41 kDa form in control mice, but primarily as the unprocessed 44 kDa form in *Rip-Pex5*$^{-/-}$ mice. **(C)** C26:0 LPC levels (n = 5 per genotype) and **(D)** plasmalogen levels (n = 4 per genotype) in islets of control and *Rip-Pex5*$^{-/-}$ mice. Data are expressed as mean ± SEM. $p < 0.05$: *; *Rip-Pex5*$^{-/-}$ versus respective control mice.

raised our interest to understand how peroxisomes contribute to the functioning of β-cells.

3.2. Generation and validation of *Rip-Pex5*$^{-/-}$ mice

We generated a tamoxifen-inducible β-cell-specific *Pex5* knockout mouse model using *Rat insulin promotor (Rip)-Cre/ER* mice [16]. The efficiency of *Pex5* deletion in pancreatic islets isolated from control and *Rip-Pex5*$^{-/-}$ mice was studied two weeks after tamoxifen induction by immunoblotting. PEX5 immunoreactivity was strongly reduced in islets of *Rip-Pex5*$^{-/-}$ as compared to control mice (Figure 1B). This resulted in impaired PEX5 function as evidenced by the presence of the 44 kDa precursor of ACAA1, whereas control islets contained the mature 41 kDa protein, which is known to be generated after import into peroxisomes (Figure 1B). The residual PEX5 immunoreactivity and peroxisomal import activity in *Rip-Pex5*$^{-/-}$ islets can be attributed to unaffected PEX5 in non-β-cells of the islets, although incomplete inactivation of PEX5 in β-cells cannot be excluded. We subsequently examined whether the loss of functional peroxisomes had an impact on peroxisomal metabolites in isolated islets. Levels of C26:0-LPC, a

sensitive marker for impaired peroxisomal β-oxidation [31,32], were 5-fold increased (Figure 1C), and plasmalogen levels were reduced by ∼35%, pointing to decreased ether lipid synthesis activity (Figure 1D). Together, these data indicate that inactivation of the *Pex5* gene in β-cells of *Rip-Pex5*$^{-/-}$ mice was successful.

3.3. Glucose tolerance and insulin secretion is impaired in *Rip-Pex5*$^{-/-}$ mice

We then assessed the consequences of peroxisome inactivation on β-cell functioning in mice either fed normal chow or a HFD diet for a period of 12 weeks, starting one week after the last tamoxifen injection. Body weights of *Rip-Pex5*$^{-/-}$ mice were not significantly different from control mice on either diet (Figure 2A and D). However, the blood glucose levels were significantly elevated in *Rip-Pex5*$^{-/-}$ mice on either diet, in the fed (Figure 2B and E) as well as in the fasted state (Figure 2C and F), indicative of impaired glucose homeostasis. To further assess glucose tolerance, an IPGTT was performed. As expected, HFD feeding induced metabolic stress in both genotypes as evident from an increased AUC (Figure 2H) as compared to the
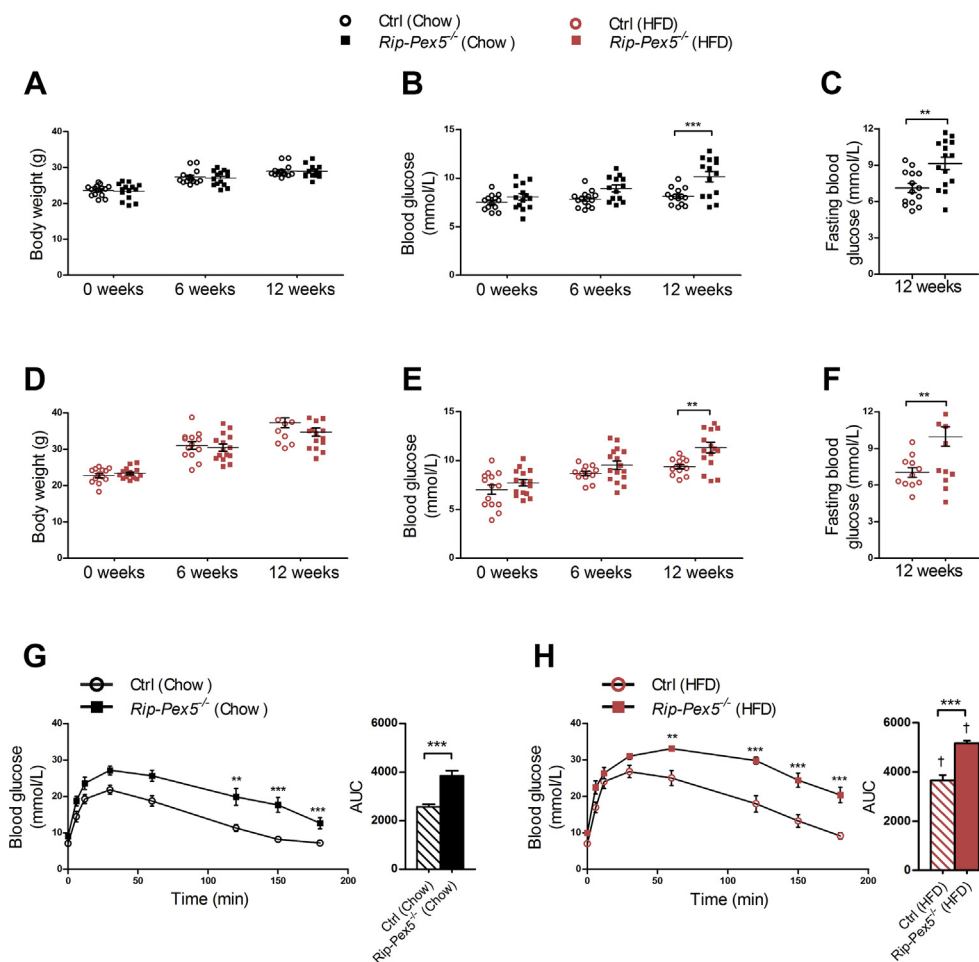
Figure 2: *Pex5* ablation in β-cells causes impaired glucose homeostasis in mice. (**A**, **D**) Body weights, (**B**, **E**) fed state blood glucose levels, and (**C**, **F**) fasting blood glucose levels of tamoxifen-treated control and *Rip-Pex5*$^{-/-}$ mice supplemented with either normal chow or HFD for 12 weeks (n = 13−16 per group). (**G**, **H**) Blood glucose and AUC measurements of IPGTT performed in control and *Rip-Pex5*$^{-/-}$ mice supplemented with either normal chow or HFD for 12 weeks (n = 13−16 per group). Data are expressed as mean ± SEM. p < 0.01: **; p < 0.001: *** *Rip-Pex5*$^{-/-}$ versus respective control mice. p < 0.001: † HFD-fed control and *Rip-Pex5*$^{-/-}$ mice versus chow-fed control and *Rip-Pex5*$^{-/-}$ mice, respectively.

respective genotype on chow diet (Figure 2G). Glucose tolerance was significantly impaired in *Rip-Pex5*$^{-/-}$ mice on both diets, with a significant increase in AUC as compared to their respective controls (Figure 2G, H).

It was previously shown that several pancreas-specific *Cre* driver lines exhibit islet dysfunction and impaired insulin secretion, even in the absence of genes targeted by loxP sites [17,23]. To exclude that the tamoxifen-inducible CRE/ER fusion protein is the source of the glucose intolerance in *Rip-Pex5*$^{-/-}$ mice, we tested Tg (Ins2-cre/ERT)^{1Dam} mice in the same study protocol of tamoxifen injection, followed by 12 weeks on HFD. No abnormalities in fasted or fed blood glucose levels, nor in IPGTT, were observed in *Rip-Cre*$^+$*Pex5*$^{WT/WT}$ and *Rip-Cre*$^+$*Pex*$^{WT/FL}$ versus *Pex5*$^{WT/WT}$, *Pex5*$^{FL/FL}$, and *Pex5*$^{WT/FL}$ mice (Supplementary Figure 1; data not shown). This excluded the role of the CRE/ER fusion protein in the observed phenotype, and therefore, *Rip-Pex5*$^{-/-}$ mice were compared with *Pex5*$^{FL/FL}$ mice in all subsequent studies.

Next, we assessed whether the impaired glucose homeostasis in *Rip-Pex5*$^{-/-}$ mice was related to abnormal plasma insulin levels in the samples collected just before starting the IPGTT as well as after 6 and 12 min of glucose injection. Control mice on either diet responded

physiologically with higher circulating insulin, whereas *Rip-Pex5*$^{-/-}$ mice were unable to do so although a significant difference with controls was observed only upon high-fat feeding (Figure 3A, B). Although it is most likely that impaired glucose homeostasis in *Rip-Pex5*$^{-/-}$ mice solely originates from changes in the pancreatic β-cells, we investigated peripheral insulin signaling by performing an IPITT. No significant differences were observed in the AUC of blood glucose levels in *Rip-Pex5*$^{-/-}$ mice as compared to control mice fed either chow or HFD (Supplementary Figure 2).

3.4. Glucose-stimulated insulin secretion and β-cell expansion is impaired in HFD-fed *Rip-Pex5*$^{-/-}$ mice

The defect in insulin secretion upon glucose stimulation in *Rip-Pex5*$^{-/-}$ mice could be due to reduced insulin content in the pancreas, reduced GSIS or a combination of both. In order to investigate the insulin secretion capacity in response to high glucose levels, *ex vivo* GSIS was performed in islets isolated from control and *Rip-Pex5*$^{-/-}$ mice fed either normal chow or HFD. A high-glucose challenge induced insulin secretion in both control and *Rip-Pex5*$^{-/-}$ mice. However, the insulin secretion (or stimulation index) upon glucose challenge was significantly reduced in *Rip-Pex5*$^{-/-}$ mice in both dietary conditions (Figure 3C, D).
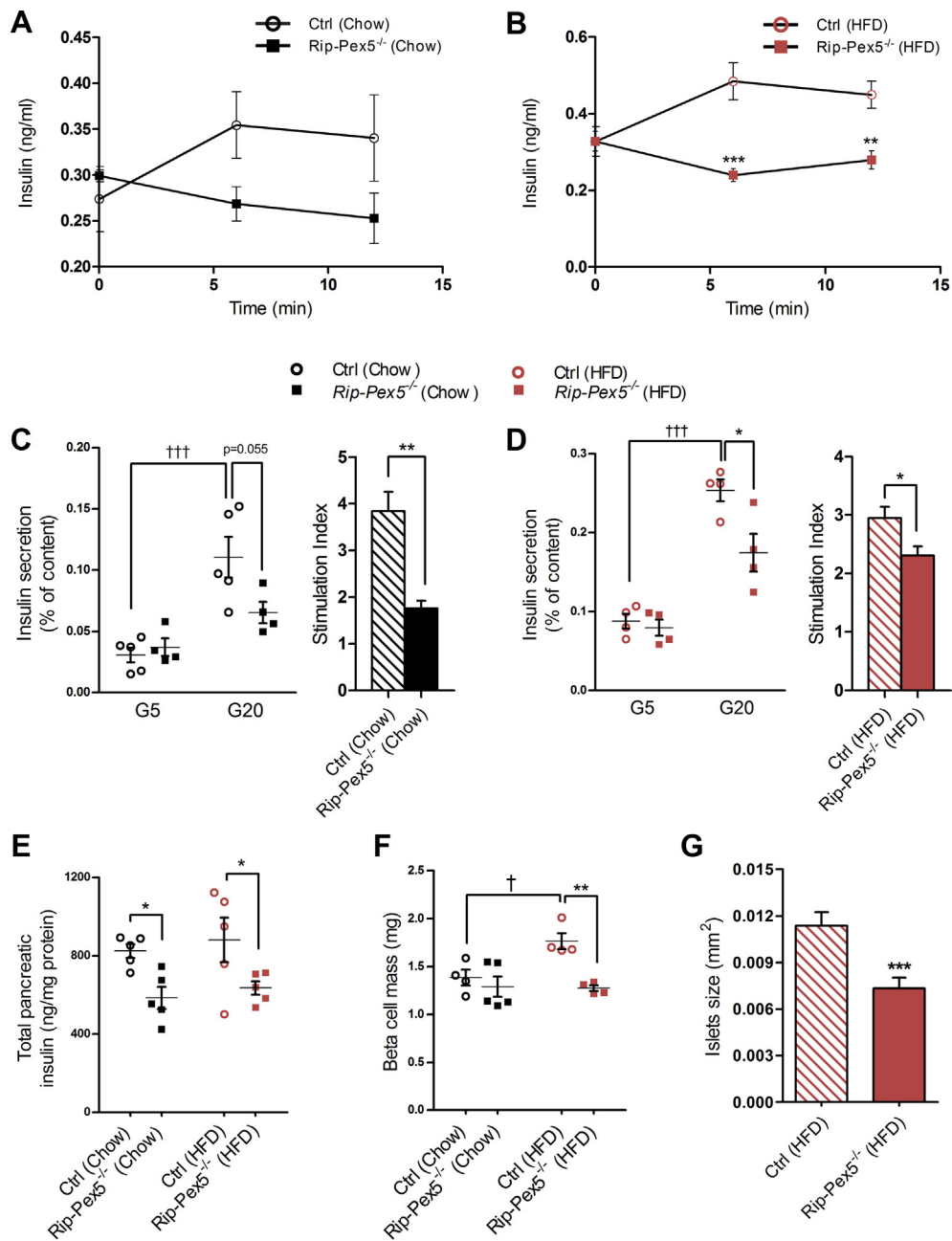
Figure 3: Glucose-stimulated insulin secretion is impaired in *Rip-Pex5*^{−/−} mice. (**A**, **B**) Plasma insulin levels in response to a glucose bolus in control and *Rip-Pex5*^{−/−} mice supplemented with either chow (n = 4) or HFD (n = 5). (**C**, **D**) Insulin secretion in response to glucose was measured *ex vivo* using islets from control and *Rip-Pex5*^{−/−} mice supplemented with either normal chow or HFD for 12 weeks (n = 4−5 per group; 50 islets per mouse). Data are presented both as % insulin released from total content and as stimulation index. (**E**) Pancreatic insulin content measurements in both chow and HFD-fed control and *Rip-Pex5*^{−/−} mice (n = 5). (**F**) β-cell mass of chow and HFD-fed control and *Rip-Pex5*^{−/−} mice (n = 4 per group). (**G**) Pancreatic islet size measurements of HFD-fed control and *Rip-Pex5*^{−/−} mice (n = 9 per group; 15−25 islets per mouse). All values are expressed as mean ± SEM. $p < 0.05$: [†]; $p < 0.001$: ^{†††} HFD-fed control versus chow-fed controls. $p < 0.05$: *; $p < 0.01$: **; $p < 0.001$: *** *Rip-Pex5*^{−/−} versus respective control mice.

Furthermore, the total pancreatic insulin content was measured using ELISA. *Rip-Pex5*^{−/−} mice contained significantly lower levels of total pancreatic insulin compared to controls on both diets (Figure 3E). To further assess whether the reduced pancreatic insulin content is accompanied by a reduction in total β-cell mass, morphometry analysis was performed on sections throughout the pancreas of control and *Rip-Pex5*^{−/−} mice stained with insulin antibodies. The analyses revealed no difference in β-cell mass between chow-fed *Rip-Pex5*^{−/−} and control

mice. In line with previous findings [33], the β-cell mass of control mice significantly increased following the metabolic stress induced by the HFD. However, *Rip-Pex5*^{−/−} mice fed HFD failed to show such compensatory increase in β-cell mass (Figure 3F). Moreover, the islets from HFD-fed *Rip-Pex5*^{−/−} mice exhibited smaller size as compared to HFD-fed control mice, as determined by mean area quantification on insulin-stained sections (Figure 3G). Taken together, these observations suggest that β-cells of *Rip-Pex5*^{−/−} mice failed to respond to elevated

glucose levels and were unable to respond to HFD-induced metabolic stress by increasing β-cell mass.

3.5. *Pex5⁻/⁻* β-cells show impaired survival

Subsequently, we investigated whether changes at the transcriptome level could unveil cellular deregulations underlying the observed anomalies of *in vivo* insulin content and secretion by performing RNAseq analysis on isolated islets from HFD-fed mice. The 3-dimensional distribution profile obtained by principal component analysis (PCA) of the variance for each gene revealed that *Rip-Pex5⁻/⁻* islets grouped separately from control islets, indicating differences in the molecular profile of these knockout β-cells (Figure 4A). A volcano plot of the combined expression data of all transcripts grouped by fold change difference and *P* values (Figure 4B) confirmed the results of the PCA analysis. Using a fold change cutoff of 2 and an adjusted *p*-value cutoff of 0.05, 497 genes (325 up-regulated and 172 down-regulated) were differentially expressed in *Rip-Pex5⁻/⁻* mice. In the entire set of differentially expressed genes (DEGs), many B-cell specific genes were represented such as immunoglobulin heavy and kappa variable fragments, and these were considered irrelevant. However, we identified a limited number of genes that are of interest (Figure 4C). The dramatic upregulation of the *Esr1* gene was likely due to the presence of the estrogen receptor in the transgenic *Cre/ER* construct. Interestingly, *Pex5* deletion from pancreatic β-cells caused the up-regulation of genes such as *Cdkn1a* [34], *Pmaip11* [35], *Pidd1* [36], *Txnip* [37], *Pitgs* [38], and *Thbs2* [39], which play a critical role in promoting apoptosis or β-cell dysfunction. However, the expression levels of *Sfrp1* [40] and *Alox5* [41], which have been reported to exert an anti-apoptotic effect and promoting insulin secretion in β-cells, respectively, were also enhanced in islets of *Rip-Pex5⁻/⁻* mice. This may be considered as a compensatory mechanism activated in response to enhanced apoptosis and reduced insulin secretion. In comparison to controls, the mRNA expression levels of *Tnfsf10 and Foxm1*, two proteins that respectively increase β-cell survival [42] and maintain normal β-cell mass [43], were significantly down-regulated in *Rip-Pex5⁻/⁻* mice. *Vnn1*, an enzyme important in maintaining islet cell homeostasis [44], was also significantly down-regulated in *Rip-Pex5⁻/⁻* mice as compared to controls (Figure 4C). Together these results suggest that loss of functional peroxisomes impacts on β-cell survival. In addition, a significant increase in mRNA levels of voltage-dependent potassium channels and chemokines was observed (Supplementary Figure 3). Because pathway analysis can reveal more marginal expression changes of the constituent genes, we applied GSEA using the KEGG database. Enrichment analysis of DEGs in the functional class of cellular processes revealed that genes were primarily enriched in "phagosome", "p53 signaling" and 'lysosome' pathways (Figure 4D). To validate the gene expression data, we first performed immunofluorescence staining of pancreatic sections to evaluate the extent of proliferation and apoptosis of β-cells in *Rip-Pex5⁻/⁻* mice. Double stainings of insulin were performed with either the proliferation marker Ki-67 or with the TUNEL assay to assess β-cell apoptosis. As shown in Figure 5A, the percentage of TUNEL-positive β-cells was significantly increased in *Rip-Pex5⁻/⁻* mice as compared to control mice. In contrast, no significant differences were observed in the number of proliferating β-cells between the groups (Figure 5B). To exclude the possibility that the observed increase in apoptosis is merely caused by hyperglycemia, the TUNEL assay was performed at an earlier age, 2 weeks after the last tamoxifen injection. These *Rip-Pex5⁻/⁻* mice also exhibited increased β-cell apoptosis in comparison to control mice (Supplementary Figure 5). Thus, the changes in β-cells antedate the
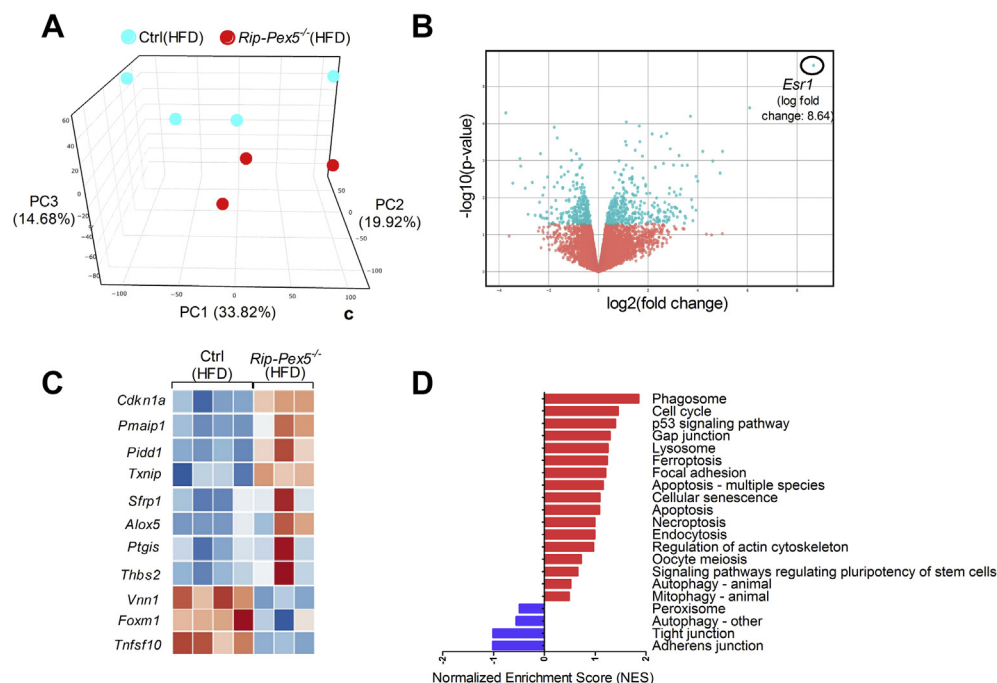

Figure 4: PEX5 ablation in β-cells affects the expression of genes associated with apoptosis. RNA-seq was performed on islets of HFD-fed *Rip-Pex5⁻/⁻* (n = 3) and control mice (n = 4). (**A**) Principal component analysis and (**B**) Volcano plot representing the RNA-seq expression data from all biological replicates of *Rip-Pex5⁻/⁻* and control mice. In the Volcano plot, blue and red indicate, respectively, the up- and down-regulated genes in *Rip-Pex5⁻/⁻* mice compared with control mice. (**C**) Heat map of differentially expressed genes (fold change > 2; p-value> 0.05) in β-cells of *Rip-Pex5⁻/⁻* mice as compared to control β-cells. Lower and higher levels of expression are presented in shades of blue and orange, respectively. (**D**) GSEA against the KEGG database showing enriched signaling pathways in β-cells of *Rip-Pex5⁻/⁻* mice.
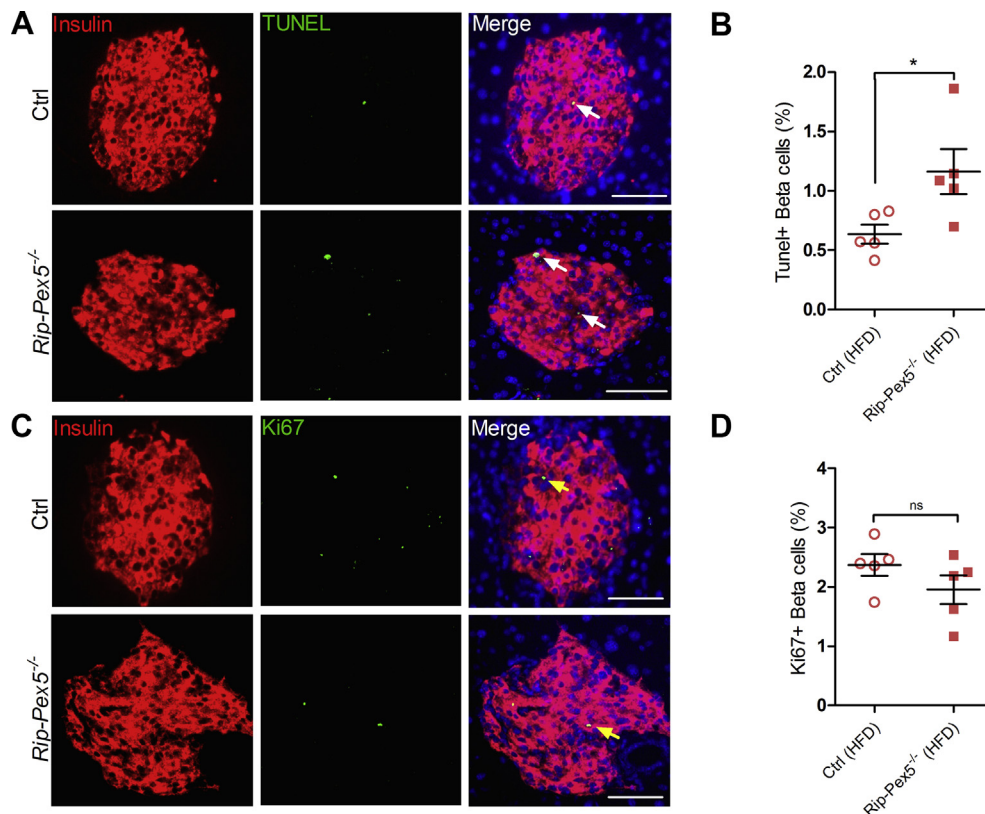
Figure 5: Assessment of β-cell apoptosis and proliferation in β-cells of *Rip-Pex5*$^{-/-}$ mice. Representative images for (**A**) TUNEL/insulin (white arrow) and (**C**) Ki67/insulin (yellow arrow) double staining of pancreatic sections from *Rip-Pex5*$^{-/-}$ and control mice. Scale bars, 50 μm. (**B, D**) Quantification of β-cell apoptosis frequency (% of β-cells analyzed) and β-cell proliferation frequency (% of β-cells analyzed) (n = 5 per genotype; 20—25 islets per mouse). Data are expressed as mean ± SEM. p < 0.05: *; *Rip-Pex5*$^{-/-}$ versus control mice.

onset of hyperglycemia and are likely a cause, rather than a consequence of it.

To evaluate the upregulated 'lysosome' pathway, we stained with LAMP2 antibodies. *Rip-Pex5*$^{-/-}$ islets stained clearly stronger for LAMP2, indicative of increased lysosomal activity (Figure 6C). Interestingly, the cells exhibiting higher LAMP2 fluorescence displayed low but detectable insulin levels (Figure 6B). Finally, in view of the role of peroxisomes in ROS metabolism [45], it is interesting to note that the RNAseq data did not indicate a deregulation of ROS signaling pathways. This was further confirmed by unaltered staining of 4-HNE (Supplementary Figure 4), a marker for increased oxidative stress [46].

3.6. *Pex5*$^{-/-}$ β-cells contain disintegrating mitochondria and translucent vacuoles

To further define the phenotype of *Pex5*-deficient β-cells, we analyzed the ultrastructure of islets from HFD fed mice by TEM. Whereas β-cells from control mice had a typical ultrastructure being highly populated with mature dense-core insulin granules (black arrow) (Figure 7A), the β-cells of *Rip-Pex5*$^{-/-}$ mice contained fewer mature insulin granules and showed an increased number of immature granules (Figure 7B). Strikingly, we observed in many (∼58%), but not in all β-cells of *Rip-Pex5*$^{-/-}$ mice an accumulation of single-membrane delimited vacuole-like structures (red arrow) that were either translucent or contained very light electrondense material (Figure 7B,C). In addition, these cells contained mitochondria (blue arrow) in which cristae had vanished to diverse extents (Figure 7B). The abundance of these abnormal mitochondria

was significantly higher in β-cells of *Rip-Pex5*$^{-/-}$ mice as compared to controls fed a HFD (Figure 7D). In order to test whether this impacted the functionality of mitochondria, complex I activity was measured. The reduction of complex I activity in islets of *Rip-Pex5*$^{-/-}$ mice compared to control mice was indicative of defective mitochondrial function (Figure 7E & Supplementary Figure 6). In view of the marked ultrastructural aberrations in HFD-fed *Rip-Pex5*$^{-/-}$ mice, we checked whether abnormalities also occur in mice fed normal chow (Figure 7F,G). Chow-fed *Rip-Pex5*$^{-/-}$ mice displayed similar albeit less prominent anomalies. The vacuole-like structures were smaller and less numerous as compared to those in HFD-fed *Rip-Pex5*$^{-/-}$ mice. Fewer mitochondria exhibited signs of degradation, but a noticeable decrease in mature insulin granules was observed (Figure 7G). Thus, loss of functional peroxisomes in β-cells is accompanied by prominent alterations in other cellular compartments, which may contribute to the impaired insulin homeostasis.

4. DISCUSSION

Peroxisomes are dynamic organelles with considerable structural and biochemical plasticity that adapt their content to cellular and environmental demands [1]. Despite decades of research, however, their specific role for the functioning of diverse cell types is still largely obscure. Here, we show that deletion of functional peroxisomes from β-cells through impeding the import of matrix proteins disrupts β-cell structure and function.
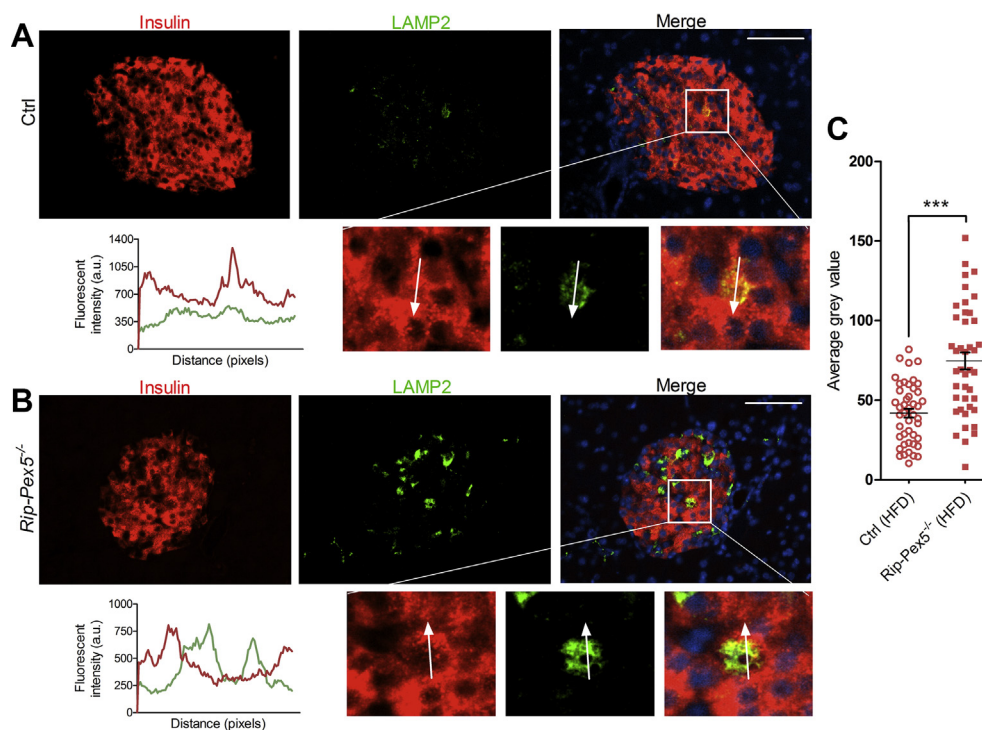
Figure 6: Expression of LAMP2 in β-cells of *Rip-Pex5*$^{-/-}$ mice. Representative islet sections of **(A)** control and **(B)** *Rip-Pex5*$^{-/-}$ mice stained for LAMP2 (green) and insulin (red). Scale bars, 100 μm. In the enlargement and in the fluorescence intensity plots, it is shown that strong LAMP2 staining in *Pex5*$^{-/-}$ islets occurs in cells containing low levels of insulin. **(C)** Quantification of mean intensity of LAMP2 in control and *Rip-Pex5*$^{-/-}$ mice (n = 3 per genotype; 12—16 islets per mouse). Data are expressed as mean ± SEM. p < 0.001: ***; *Rip-Pex5*$^{-/-}$ versus control mice. a.u., arbitrary units.

In comparison to the exocrine pancreas, we found that the abundance of peroxisomes in islets was very high, pointing to particular roles of these organelles in the endocrine cells. This is likely not related to an anti-oxidant function as it is well established that catalase expression in β- and α-cells is notoriously low [47]. Catalase is indeed one of the 'forbidden' genes [9,48] in mouse pancreatic islet tissue but the significance of this profound repression of mRNA abundance for β-cell functioning is not clear. Lentiviral-mediated overexpression of catalase, either in the cytosol or in mitochondria, did not affect glucose-stimulated insulin secretion in rat islets [11]. However, elevating the levels of catalase in its normal cellular context i.e. in peroxisomes was not attempted. The precise role of ROS signaling for β-cell function has still not been elucidated. According to data from Elsner et al. [14], the production of peroxisomal H$_2$O$_2$, a side product formed during the first step of peroxisomal β-oxidation, is toxic for rat β-cells. Differences between saturated and unsaturated fatty acids [49] and between rat and human [50] were subsequently reported, which cannot be explained by our current understanding of peroxisomal β-oxidation. Peroxisomes play a pivotal role in cellular ROS homeostasis, but the consequences of the ectopic localization of both the ROS generating and degrading enzymes are unpredictable and could depend on the cell type. In *Rip-Pex5*$^{-/-}$ mice, we did not find evidence for increased ROS and it is therefore unlikely that aberrant redox signaling is responsible for the observed phenotype. Instead, the high peroxisomal abundance in β-cells and the cellular aberrations caused by their absence are probably related to the role of peroxisomes in lipid metabolism. Deletion of peroxisomal matrix import protein resulted both in increased levels of very long chain fatty acids due to a defect in β-oxidation and in a reduction of plasmalogens due to impaired ether lipid synthesis. Which of these or possibly other metabolic derangements contribute to the observed phenotype remains to be investigated. In this respect, it is interesting to note that a mild reduction in phoshatidylcholine plasmalogen species, but not in the more abundant phosphatidylethanolamine plasmalogens, was found following stimulation of murine pancreatic islets with glucose [52]. The most prominent alterations in β-cells were degenerative features of mitochondria and an accumulation of vacuole-like structures. Mitochondrial alterations as a consequence of defective peroxisomal function were previously reported but were strongly dependent on the cell type and nature of the peroxisomal dysfunction. Mitochondrial destruction was most prominent in *Pex5*-deficient hepatocytes, with sparse and unusually shaped cristae and a severe reduction of complex I activity [51]. Other complexes were less (complex III and V) or not affected (complex II and IV) [51]. In contrast no obvious functional nor structural mitochondrial impairments were seen in *Pex5*-deleted striated muscle and brain [53]. In *Pex5*-deficient β-cells, several mitochondria were found in which the cristae structure seemed to be gradually lost, ultimately impacting complex I activity. In addition, in the majority but not in all β-cells, an accumulation of vesicles with a low electron density and surrounded by a single membrane was observed. Such structures were not seen in other *Pex5*-deficient cell types (hepatocytes, neural cells, striated muscle) [51,53]. We could not define the origin and nature of these vacuole-like structures but in view of their size, they are not compatible with peroxisomal ghosts [54]. Cytoplasmic vacuolization, a well-known morphological phenomenon observed in mammalian cells in response to viral or toxic inducers, has been implicated in various forms of cell death [55]. Vacuoles can originate from several components of the endo-lysosomal system. Interestingly, such structures of undefined origin were also seen in β-
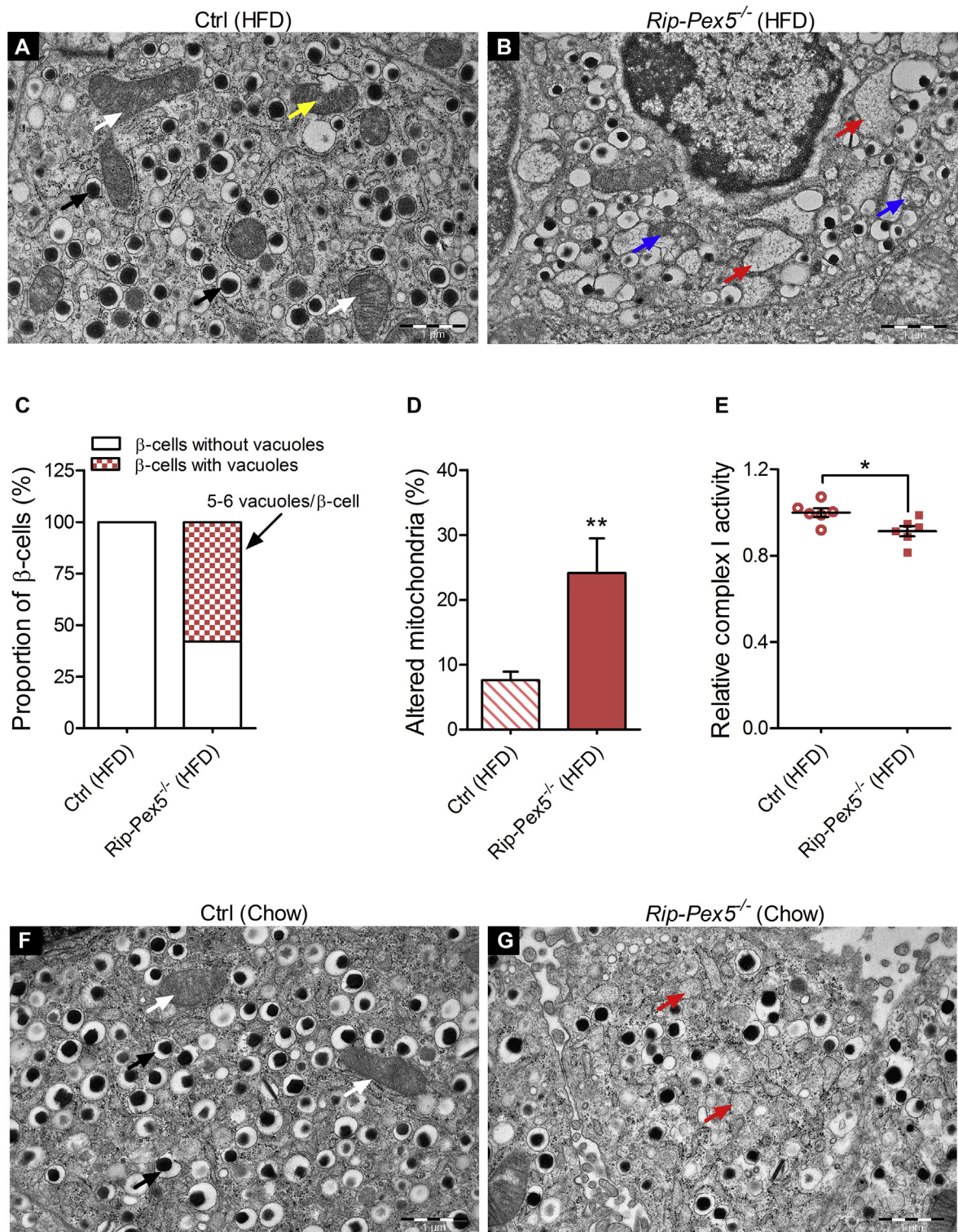
Figure 7: Loss of PEX5 in β-cells causes mitochondrial deterioration and massive vacuole overload. Representative electron micrographs of (**A**) HFD-fed control β-cells showing normal (white arrow) and slightly damaged mitochondria (yellow arrow) and numerous electron dense insulin granules (black arrow), whereas (**B**) HFD-fed *Rip-Pex5*$^{-/-}$ mice showed marked changes in β-cells represented by damaged mitochondria (blue arrow), reduced numbers of mature secretory granules, and cytoplasmic vacuolization (red arrow). n = 3—4 per group; Scale bars, 1 μm. (**C**) Stacked box plot showing the proportion of β-cells having vacuole-like structures (along with the number of vacuoles per β-cell) in HFD-fed *Rip-Pex5*$^{-/-}$ and control mice. (**D**) Graph showing the percentage of altered mitochondria in β-cells from HFD-fed control and *Rip-Pex5*$^{-/-}$ mice. (**E**) Relative complex I activity in islets isolated from HFD-fed control and *Rip-Pex5*$^{-/-}$ mice (n = 6 per genotype). (**F, G**) Representative electron micrographs of chow-fed control and *Rip-Pex5*$^{-/-}$ β-cells showing reduced numbers of mature secretory granules and cytoplasmic vacuolization (red arrow, more pronounced in HFD-fed *Rip-Pex5*$^{-/-}$ mice (**B**)). n = 3 per group; Scale bars, 1 μm. Data are expressed as mean ± SEM. $p < 0.05$: *; $p < 0.01$: **; *Rip-Pex5*$^{-/-}$ versus control mice.

cells from type 2 diabetes patients and in murine β-cells in which the autophagic process was hyperactivated [56,57] and in a model in which Cdk4/6 inhibition caused pancreatic β-cell loss and glucose deregulation [58].

Interestingly, pathway enrichment analysis of the transcriptome of *Rip-Pex5$^{-/-}$* islets revealed a positive correlation with the 'lysosome' pathway, which was supported by increased LAMP2 immunoreactivity. A recent study by Kleinecke et al. also suggested that peroxisome dysfunction has severe consequences on the function of lysosomes [59]. However, additional research is needed to better understand the link between peroxisomes and lysosomes in β-cells. Also, other transcriptome changes in *Rip-Pex5$^{-/-}$* islets that are of potential interest require further analysis to understand their contribution to the phenotype. For example, increased expression of voltage-dependent potassium channels might affect β-cell electrical activity and insulin secretion [60]. On the other hand, an increased expression of chemokines may cause immune cell recruitment and β-cell dysfunction [61].

It is interesting to note that all the ultrastructural changes were more prominent in HFD-fed *Rip-Pex5$^{-/-}$* mice, but they also occurred in mice fed normal chow. This indicates that peroxisomes are needed to maintain β-cells under basal conditions, but might play a more crucial role in situations of metabolic stress. The structural anomalies of β-cells in *Rip-Pex5$^{-/-}$* mice were accompanied by a deregulation of glucose homeostasis. Glucose levels were significantly elevated in fed and fasting conditions, although they did not reach diabetic levels. This was likely due to impaired insulin secretion as observed in response to a bolus of glucose both *in vivo* and *ex vivo*. *Rip-Pex5$^{-/-}$* mice also exhibited a significant reduction in total pancreatic insulin content on both diets, whereas the β-cell mass was only reduced in the HFD condition. Hence, peroxisome deficient β-cells fail to show a compensatory increase when exposed to a continuous overload of lipids. This observation supports the proposition that peroxisomes are particularly needed to adapt β-cell mass during conditions of metabolic stress. Transcriptome analysis revealed that several genes involved in apoptosis were upregulated in β-cells of *Rip-Pex5$^{-/-}$* mice. This was further confirmed by an increase in TUNEL staining whereas proliferation markers were unaltered. Thus, the decrease in β-cell mass is rather caused by increased apoptosis of β-cells and not by impaired proliferation.

The β-cell deregulation could be a direct consequence of altered levels of peroxisomal metabolites, but the secondary cellular alterations, and in particular the degeneration of an important fraction of mitochondria, could be involved as well. In order to decipher how the loss of peroxisomal activity in β-cells interferes with other cellular compartments, including mitochondria and the endolysosomal system, and results in increased apoptotic cell death, it would be instructive to eliminate PEX5 in an insulinoma cell line. Provided that the cellular anomalies are recapitulated *in vitro*, this would allow to define the sequence of cellular events and to stimulate or block processes, such as the endolysosomal pathway.

It also remains to be investigated whether the findings in mice can be translated to men. In patients with peroxisome biogenesis disorders, glucose homeostasis has not been well documented. Severely affected patients have feeding difficulties due to hypotonia and usually do not live up to one year of age, hence they are not exposed to lipid overload. On the other hand, the longer-surviving patients have mild mutations which may not lead to β-cell dysfunction. Ageing has been related to reduced peroxisomal function, and it remains to be investigated whether this could impact on β-cell function, in particular in conditions of metabolic overload.

5. CONCLUSIONS

In conclusion, this study was performed in response to long-standing open questions on how peroxisomes contribute to β-cell function. Our data provide evidence that peroxisomal metabolism plays an essential role in the preservation of β-cell integrity. Although we cannot exclude the involvement of other cell types, this likely occurs in a cell autonomous way. This suggests that enhancing peroxisome activity is a potential avenue to support β-cell function in metabolic stress conditions.

CONTRIBUTION STATEMENT

RKB, ABS, MB, and PVV contributed to the conception and design of the study. RKB, ABS, KL, and PVV were involved with data acquisition. RKB, ABS, FS, PVV, MF, and MB performed data analysis and interpretation. RKB, ABS, and MB drafted the manuscript. All authors contributed to critically revising the article for important intellectual content and gave their final approval of the version to be published.

CONFLICT OF INTEREST

The authors declare no conflict of interest associated with this manuscript.

APPENDIX A. SUPPLEMENTARY DATA

Supplementary data to this article can be found online at https://doi.org/10.1016/j.molmet.2019.02.001.

REFERENCES

[1] Islinger, M., Voelkl, A., Fahimi, H.D., Schrader, M., 2018. The peroxisome: an update on mysteries 2.0. Histochemistry and Cell Biology 150(5):443—471. https://doi.org/10.1007/s00418-018-1722-1725.

[2] Wanders, R.J.A., 2014. Metabolic functions of peroxisomes in health and disease. Biochimie 98:36—44. https://doi.org/10.1016/j.biochi.2013.08.022.

[3] Dixit, E., Boulant, S., Zhang, Y., Lee, A.S.Y., Odendall, C., Shum, B., et al., 2010. Peroxisomes are signaling platforms for antiviral innate immunity. Cell 141(4):668—681. https://doi.org/10.1016/j.cell.2010.04.018.

[4] Fransen, M., Lismont, C., Walton, P., 2017. The peroxisome-mitochondria connection: how and why? International Journal of Molecular Sciences 18(6):1126 https://doi.org/10.3390/ijms18061126.

[5] Castro, I.G., Schuldiner, M., Zalckvar, E., 2018. Mind the organelle gap — peroxisome contact sites in disease. Trends in Biochemical Sciences 43(3): 199—210. https://doi.org/10.1016/j.tibs.2018.01.001.

[6] Costello, J.L., Castro, I.G., Hacker, C., Schrader, T.A., Metz, J., Zeuschner, D., et al., 2017. ACBD5 and VAPB mediate membrane associations between

peroxisomes and the ER. The Journal of Cell Biology 216(2):331—342. https://doi.org/10.1083/jcb.201607055.

[7] Lenzen, S., Drinkgern, J., 1996. Low antioxidant enzyme gene expression in pancreatic islets compared with various other mouse tissues. Free Radical Biology and Medicine 20(3):463—466. https://doi.org/10.1016/0891-5849(96)02051-5.

[8] Thorrez, L., Laudadio, I., Van Deun, K., Quintens, R., Hendrickx, N., Granvik, M., et al., 2011. Tissue-specific disallowance of housekeeping genes: the other face of cell differentiation. Genome Research 21(1):95—105. https://doi.org/10.1101/gr.109173.110.

[9] Pullen, T.J., Rutter, G.A., 2013. When less is more: the forbidden fruits of gene repression in the adult beta-cell. Diabetes, Obesity and Metabolism 15(6):503—512. https://doi.org/10.1111/dom.12029.

[10] Lemaire, K., Thorrez, L., Schuit, F., 2016. Disallowed and allowed gene expression: two faces of mature islet beta cells. Annual Review of Nutrition 36:45—71. https://doi.org/10.1146/annurev-nutr-071715-050808.

[11] Lortz, S., Gurgul-Convey, E., Naujok, O., Lenzen, S., 2013. Overexpression of the antioxidant enzyme catalase does not interfere with the glucose responsiveness of insulin-secreting INS-1E cells and rat islets. Diabetologia 56(4):774—782. https://doi.org/10.1007/s00125-012-2823-7.

[12] Góth, L., Eaton, J.W., 2000. Hereditary catalase deficiencies and increased risk of diabetes. Lancet 356(9244):1820—1821. https://doi.org/10.1016/S0140-6736(00)03238-4.

[13] Fontés, G., Zarrouki, B., Hagman, D.K., Latour, M.G., Semache, M., Roskens, V., et al., 2010. Glucolipotoxicity age-dependently impairs beta cell function in rats despite a marked increase in beta cell mass. Diabetologia 53(11):2369—2379. https://doi.org/10.1007/s00125-010-1850-5.

[14] Elsner, M., Gehrmann, W., Lenzen, S., 2011. Peroxisome-generated hydrogen peroxide as important mediator of lipotoxicity in insulin-producing cells. Diabetes 60(1):200—208. https://doi.org/10.2337/db09-1401.

[15] Hellemans, K., Kerckhofs, K., Hannaert, J.-C., Martens, G., Van Veldhoven, P., Pipeleers, D., 2007. Peroxisome proliferator-activated receptor alpha-retinoid X receptor agonists induce beta-cell protection against palmitate toxicity. The FEBS Journal 274(23):6094—6105. https://doi.org/10.1111/j.1742-4658.2007.06131.x.

[16] Dor, Y., Brown, J., Martinez, O.I., Melton, D.A., 2004. Adult pancreatic β-cells are formed by self-duplication rather than stem-cell differentiation. Nature 429:41.

[17] Lee, J.Y., Ristow, M., Lin, X., White, M.F., Magnuson, M.A., Hennighausen, L., 2006. RIP-Cre revisited, evidence for impairments of pancreatic β-cell function. Journal of Biological Chemistry 281(5):2649—2653. https://doi.org/10.1074/jbc.M512373200.

[18] Lemaire, K., Ravier, M.A., Schraenen, A., Creemers, J.W.M., Van de Plas, R., Granvik, M., et al., 2009. Insulin crystallization depends on zinc transporter ZnT8 expression, but is not required for normal glucose homeostasis in mice. Proceedings of the National Academy of Sciences of the United States of America 106(35):14872—14877. https://doi.org/10.1073/pnas.0906587106.

[19] Cheng, Q., Boucher, B.J., Leung, P.S., 2013. Modulation of hypovitaminosis D-induced islet dysfunction and insulin resistance through direct suppression of the pancreatic islet renin—angiotensin system in mice. Diabetologia 56(3):553—562. https://doi.org/10.1007/s00125-012-2801-0.

[20] Lalloyer, F., Vandewalle, B., Percevault, F., Torpier, G., Kerr-Conte, J., Oosterveer, M., et al., 2006. Peroxisome proliferator—activated receptor α improves pancreatic adaptation to insulin resistance in obese mice and reduces lipotoxicity in human islets. Diabetes 55(6). https://doi.org/10.2337/db06-0016, 1605 LP-1613.

[21] Amery, L., Fransen, M., De Nys, K., Mannaerts, G.P., Van Veldhoven, P.P., 2000. Mitochondrial and peroxisomal targeting of 2-methylacyl-CoA racemase in humans. Journal of Lipid Research.

[22] Antonenkov, V.D., Van Veldhoven, P.P., Waelkens, E., Mannaerts, G.P., 1997. Substrate Specificities of 3-oxoacyl-CoA thiolase A and sterol carrier protein 2/3-oxoacyl-CoA thiolase purified from normal rat liver peroxisomes: sterol carrier protein 2/3-oxoacyl-CoA thiolase is involved in the metabolism of 2-methyl-branched fatty acids and bile acid intermediates. Journal of Biological Chemistry 272(41):26023—26031. https://doi.org/10.1074/jbc.272.41.26023.

[23] Brouwers, B., De Faudeur, G., Osipovich, A.B., Goyvaerts, L., Lemaire, K., Boesmans, L., et al., 2014. Impaired islet function in commonly used transgenic mouse lines due to human growth hormone minigene expression. Cell Metabolism 20(6):979—990. https://doi.org/10.1016/j.cmet.2014.11.004.

[24] Natale, G., Lenzi, P., Lazzeri, G., Falleni, A., Biagioni, F., Ryskalin, L., et al., 2015. Compartment-dependent mitochondrial alterations in experimental ALS, the effects of mitophagy and mitochondriogenesis. Frontiers in Cellular Neuroscience 9. https://doi.org/10.3389/fncel.2015.00434.

[25] Van De Beek, M.C., Dijkstra, I.M.E., Van Lenthe, H., Ofman, R., Goldhaber-Pasillas, D., Schauer, N., et al., 2016. C26:0-Carnitine is a new biomarker for X-linked adrenoleukodystrophy in mice and man. PLoS One 11(4):e0154597. https://doi.org/10.1371/journal.pone.0154597.

[26] Van Veldhoven, P.P., Mannaerts, G.P., 1987. Inorganic and organic phosphate measurements in the nanomolar range. Analytical Biochemistry 161(1):45—48. https://doi.org/10.1016/0003-2697(87)90649-X.

[27] Mezzar, S., de Schryver, E., Van Veldhoven, P.P., 2014. RP-HPLC-fluorescence analysis of aliphatic aldehydes: application to aldehyde-generating enzymes HACL1 and SGPL1. Journal of Lipid Research 55(3):573—582. https://doi.org/10.1194/jlr.D044230.

[28] Dodt, G., Braverman, N., Wong, C., Moser, A., Moser, H.W., Watkins, P., et al., 1995. Mutations in the PTS1 receptor gene, PXR1, define complementation group 2 of the peroxisome biogenesis disorders. Nature Genetics 9(2):115—125. https://doi.org/10.1038/ng0295-115.

[29] Bray, N.L., Pimentel, H., Melsted, P., Pachter, L., 2016. Near-optimal probabilistic RNA-seq quantification. Nature Biotechnology 34(5):524—527. https://doi.org/10.1038/nbt.3519.

[30] Robinson, M.D., McCarthy, D.J., Smyth, G.K., 2010. edgeR: a Bioconductor package for differential expression analysis of digital gene expression data. Bioinformatics 26(1):139—140. https://doi.org/10.1093/bioinformatics/btp616.

[31] Turgeon, C.T., Moser, A.B., Mørkrid, L., Magera, M.J., Gavrilov, D.K., Oglesbee, D., et al., 2015. Streamlined determination of lysophosphatidylcholines in dried blood spots for newborn screening of X-linked adrenoleukodystrophy. Molecular Genetics and Metabolism 114(1):46—50. https://doi.org/10.1016/j.ymgme.2014.11.013.

[32] Klouwer, F.C.C., Ferdinandusse, S., van Lenthe, H., Kulik, W., Wanders, R.J.A., Poll-The, B.T., et al., 2017. Evaluation of C26:0-lysophosphatidylcholine and C26:0-carnitine as diagnostic markers for Zellweger spectrum disorders. Journal of Inherited Metabolic Disease 40(6):875—881. https://doi.org/10.1007/s10545-017-0064-0.

[33] Golson, M.L., Misfeldt, A.A., Kopsombut, U.G., Petersen, C.P., Gannon, M., 2010. High fat diet regulation of β-cell proliferation and β-cell mass. The Open Endocrinology Journal 4. https://doi.org/10.2174/1874216501004010066.

[34] Gartel, A.L., Radhakrishnan, S.K., 2005. Lost in transcription: p21 repression, mechanisms, and consequences. Cancer Research, 3980—3985. https://doi.org/10.1158/0008-5472.CAN-04-3995.

[35] Villunger, A., Michalak, E.M., Coultas, L., Müllauer, F., Böck, G., Ausserlechner, M.J., et al., 2003. p53- and drug-induced apoptotic responses mediated by BH3-only proteins puma and noxa. Science 302(5647):1036—1038. https://doi.org/10.1126/science.1090072.

[36] Lin, Y., Ma, W., Benchimol, S., 2000. Pidd, a new death-domain-containing protein, is induced by p53 and promotes apoptosis. Nature Genetics 26(1):122—125. https://doi.org/10.1038/79102.

[37] Xu, G., Chen, J., Jing, G., Shalev, A., 2013. Thioredoxin-interacting protein regulates insulin transcription through microRNA-204. Nature Medicine 19(9):1141—1146. https://doi.org/10.1038/nm.3287.

 www.molecularmetabolism.com

[38] Luo, P., Wang, M.-H., 2011. Eicosanoids, β-cell function, and diabetes. Prostaglandins & Other Lipid Mediators 95(1–4):1–10. https://doi.org/10.1016/j.prostaglandins.2011.06.001.

[39] Lopes, N., Gregg, D., Vasudevan, S., Hassanain, H., Goldschmidt-Clermont, P., Kovacic, H., 2003. Thrombospondin 2 regulates cell proliferation induced by Rac1 redox-dependent signaling. Molecular and Cellular Biology 23(15):5401–5408. https://doi.org/10.1128/MCB.23.15.5401.

[40] Han, X., Amar, S., 2004. Secreted frizzled-related protein 1 (SFRP1) protects fibroblasts from ceramide-induced apoptosis. Journal of Biological Chemistry 279(4):2832–2840. https://doi.org/10.1074/jbc.M308102200.

[41] Mehrabian, M., Schulthess, F.T., Nebohacova, M., Quiros, M.A., Castellani, L.W., Zhou, Z., et al., 2008. Identification of 5-lipoxygenase as a gene regulating adiposity and pancreatic function. Diabetologia 51(6):978–988. https://doi.org/10.1007/s00125-008-1002-3.

[42] Kahraman, S., Dirice, E., Altunbas, H.A., Şanlıoğlu, A.D., 2014. Proliferative effect of sTRAIL on mouse pancreatic beta cells. Journal of the Pancreas 540. https://doi.org/10.6092/1590-8577%2F2790.

[43] Zhang, H., Ackermann, A.M., Gusarova, G. a., Lowe, D., Feng, X., Kopsombut, U.G., et al., 2006. The FoxM1 transcription factor is required to maintain pancreatic beta-cell mass. Molecular Endocrinology (Baltimore, Md.) 20(8):1853–1866. https://doi.org/10.1210/me.2006-0056.

[44] Roisin-Bouffay, C., Castellano, R., Valéro, R., Chasson, L., Galland, F., Naquet, P., 2008. Mouse vanin-1 is cytoprotective for islet beta cells and regulates the development of type 1 diabetes. Diabetologia 51(7):1192–1201. https://doi.org/10.1007/s00125-008-1017-9.

[45] Fransen, M., Nordgren, M., Wang, B., Apanasets, O., 2012. Role of peroxisomes in ROS/RNS-metabolism: implications for human disease. Biochimica et Biophysica Acta (BBA) Molecular Basis of Disease 1822(9):1363–1373.. https://doi.org/10.1016/j.bbadis.2011.12.001.

[46] Breitzig, M., Bhimineni, C., Lockey, R., Kolliputi, N., 2016. 4-Hydroxy-2-nonenal: a critical target in oxidative stress? American Journal of Physiology Cell Physiology 311(4):C537–C543 https://doi.org/10.1152/ajpcell.00101.2016.

[47] Lemaire, K., Granvik, M., Schraenen, A., Goyvaerts, L., Van Lommel, L., Gómez-Ruiz, A., et al., 2017. How stable is repression of disallowed genes in pancreatic islets in response to metabolic stress? PLoS One 12(8):e0181651 https://doi.org/10.1371/journal.pone.0181651.

[48] Schuit, F., Van Lommel, L., Granvik, M., Goyvaerts, L., De Faudeur, G., Schraenen, A., et al., 2012. Beta-cell-specific gene repression: a mechanism to protect against inappropriate or maladjusted insulin secretion? Diabetes 61(5):969–975 https://doi.org/10.2337/db11-1564.

[49] Gehrmann, W., Würdemann, W., Plötz, T., Jörns, A., Lenzen, S., Elsner, M., 2015. Antagonism between saturated and unsaturated fatty Acids in ROS mediated lipotoxicity in rat insulin-producing cells. Cellular Physiology and Biochemistry 36(3):852–865. https://doi.org/10.1159/000430261.

[50] Plötz, T., Krümmel, B., Laporte, A., Pingitore, A., Persaud, S.J., Jörns, A., et al., 2017. The monounsaturated fatty acid oleate is the major physiological toxic free fatty acid for human beta cells. Nutrition & Diabetes 7(12):305. https://doi.org/10.1038/s41387-017-0005-x.

[51] Peeters, A., Shinde, A.B., Dirkx, R., Smet, J., De Bock, K., Espeel, M., et al., 2015. Mitochondria in peroxisome-deficient hepatocytes exhibit impaired respiration, depleted DNA, and PGC-1α independent proliferation. Biochimica et Biophysica Acta Molecular Cell Research 1853(2):285–298. https://doi.org/10.1016/j.bbamcr.2014.11.017.

[52] Pearson, G.L., Mellett, N., Chu, K.Y., Boslem, E., Meikle, P.J., Biden, T.J., 2016. A comprehensive lipidomic screen of pancreatic β-cells using mass spectroscopy defines novel features of glucose-stimulated turnover of neutral lipids, sphingolipids and plasmalogens. Molecular Metabolism 5(6):404–414. https://doi.org/10.1016/j.molmet.2016.04.003.

[53] Shinde, A.B., Baboota, R.K., Denis, S., Loizides-Mangold, U., Peeters, A., Espeel, M., et al., 2018. Mitochondrial disruption in peroxisome deficient cells is hepatocyte selective but is not mediated by common hepatic peroxisomal metabolites. Mitochondrion 39:51–59. https://doi.org/10.1016/j.mito.2017.08.013.

[54] Soliman, K., Göttfert, F., Rosewich, H., Thoms, S., Gärtner, J., 2018. Super-resolution imaging reveals the sub-diffraction phenotype of Zellweger Syndrome ghosts and wild-type peroxisomes. Scientific Reports 8(1):7809. https://doi.org/10.1038/s41598-018-24119-2.

[55] Shubin, A.V., Demidyuk, I.V., Komissarov, A.A., Rafieva, L.M., Kostrov, S.V., 2016. Cytoplasmic vacuolization in cell death and survival. Oncotarget 7(34):55863–55889. https://doi.org/10.18632/oncotarget.10150.

[56] Masini, M., Bugliani, M., Lupi, R., del Guerra, S., Boggi, U., Filipponi, F., et al., 2009. Autophagy in human type 2 diabetes pancreatic beta cells. Diabetologia 52(6):1083–1086. https://doi.org/10.1007/s00125-009-1347-2.

[57] Yamamoto, S., Kuramoto, K., Wang, N., Situ, X., Priyadarshini, M., Zhang, W., et al., 2018. Autophagy differentially regulates insulin production and insulin sensitivity. Cell Reports 23(11):3286–3299. https://doi.org/10.1016/j.celrep.2018.05.032.

[58] Sacaan, A.I., Thibault, S., Hong, M., Kondegowda, N.G., Nichols, T., Li, R., et al., 2017. CDK4/6 Inhibition on glucose and pancreatic beta cell homeostasis in young and aged Rats. Molecular Cancer Research 15(11), 1531 LP-1541.

[59] Kleinecke, S., Richert, S., de Hoz, L., Brügger, B., Kungl, T., Asadollahi, E., et al., 2017. Peroxisomal dysfunctions cause lysosomal storage and axonal Kv1 channel redistribution in peripheral neuropathy. ELife 6:e23332. https://doi.org/10.7554/eLife.23332.

[60] MacDonald, P.E., Wheeler, M.B., 2003. Voltage-dependent K+ channels in pancreatic beta cells: role, regulation and potential as therapeutic targets. Diabetologia 46(8):1046–1062. https://doi.org/10.1007/s00125-003-1159-8.

[61] Burke, S.J., Collier, J.J., 2015. Transcriptional regulation of chemokine genes: a link to pancreatic islet inflammation? Biomolecules 5(2):1020–1034 https://doi.org/10.3390/biom5021020.